

10174
NACA TN 3818



NATIONAL ADVISORY COMMITTEE FOR AERONAUTICS

TECHNICAL NOTE 3818

WIND-TUNNEL INVESTIGATION TO DETERMINE THE
HORIZONTAL- AND VERTICAL-TAIL CONTRIBUTIONS TO THE STATIC
LATERAL STABILITY CHARACTERISTICS OF A COMPLETE-MODEL
SWEPT-WING CONFIGURATION AT HIGH SUBSONIC SPEEDS

By James W. Wiggins, Richard E. Kuhn,
and Paul G. Fournier

Langley Aeronautical Laboratory
Langley Field, Va.



Washington

November 1956

AFM/C
TECHNICAL LIBRARY
AFL 2311



0066710

TECHNICAL NOTE 3818

WIND-TUNNEL INVESTIGATION TO DETERMINE THE
 HORIZONTAL- AND VERTICAL-TAIL CONTRIBUTIONS TO THE STATIC
 LATERAL STABILITY CHARACTERISTICS OF A COMPLETE-MODEL
 SWEEP-WING CONFIGURATION AT HIGH SUBSONIC SPEEDS¹

By James W. Wiggins, Richard E. Kuhn,
 and Paul G. Fournier

SUMMARY

An investigation was conducted in the Langley high-speed 7- by 10-foot tunnel to determine the horizontal- and vertical-tail contributions to the static lateral stability of a complete-model swept-wing configuration at high subsonic speeds. The results indicate that, in general, Mach number effects within the range studied and wing effects on the tail contribution were small and the overall trends of the data of the present investigation agreed with those which have been established at low speeds. The contribution of the vertical tail to the directional stability $C_{n\beta}$ at zero angle of attack increases slightly with Mach number and can be adequately predicted when the load is assumed to act at the aerodynamic center of the vertical tail $\bar{c}_v/4$ and when the end-plate effect of the fuselage on the theoretical lift-curve slope of the tail is considered. The vertical tail contributes a stabilizing increment to the directional stability $C_{n\beta}$ at all angles of attack; however, at the higher angles of attack the tail contribution is greatly reduced. The vertical-tail contribution to the effective-dihedral derivative $C_{l\beta}$ at zero angle of attack increases slightly with Mach number and can be estimated satisfactorily when the geometric center of load $\bar{c}_v/4$ and the end-plate effect of the fuselage on the theoretical lift-curve slope of the tail are considered. The rate of change of the effective-dihedral derivative with angle of attack $\frac{\partial(C_{l\beta})}{\partial\alpha}$ was greater throughout the Mach number range than calculations indicated. The end-plate effect of the fuselage on the vertical tail decreased with Mach number and indicated good agreement with low-speed data at the lowest Mach number. Interference effects of the wing and horizontal tail on the lateral-stability derivatives were small at the lower angles of attack.

¹Supersedes recently declassified NACA Research Memorandum L53E19 by James W. Wiggins, Richard E. Kuhn, and Paul G. Fournier, 1953.

INTRODUCTION

A systematic research program is being carried out in the Langley high-speed 7- by 10-foot tunnel to determine the aerodynamic characteristics of various arrangements of the component parts of research-type airplane models. Results are being obtained in pitch, sideslip, and during steady rolling up to a Mach number of 0.95.

This paper presents results of an investigation of the static lateral stability characteristics of a 45° swept-wing airplane configuration and some of its component parts. The longitudinal aerodynamic characteristics of the wing-fuselage configuration are presented in reference 1. The Reynolds number range for the model varied from 1.8×10^6 to 3.0×10^6 .

Some significant characteristics are compared with available theory and low-speed results from the Langley stability tunnel.

SYMBOLS AND COEFFICIENTS

All forces and moments are referred to the stability axes (fig. 1), with the origin at the projection on the plane of symmetry of the quarter-chord point of the mean aerodynamic chord of the wing.

C_L	lift coefficient, $\frac{\text{Lift}}{qS_W}$
C_l	rolling-moment coefficient, $\frac{\text{Rolling moment}}{qS_W b_W}$
C_n	yawing-moment coefficient, $\frac{\text{Yawing moment}}{qS_W b_W}$
C_y	lateral-force coefficient, $\frac{\text{Lateral force}}{qS_W}$
q	dynamic pressure, $\frac{\rho V^2}{2}$, lb/sq ft
V	free-stream velocity, ft/sec
ρ	mass density of air, slugs/cu ft
S	area, sq ft

b	span, ft
\bar{c}	mean aerodynamic chord, ft
α	angle of attack, deg
β	angle of sideslip, deg
M	Mach number
R	Reynolds number
η_n, η_Y	angle-of-attack correction factors to effectiveness of vertical tail in sideslip
l_V	tail length, distance from origin of axes to aerodynamic center of vertical tail measured along fuselage center line, ft
z_V	perpendicular distance from fuselage center line to aerodynamic center of vertical tail, ft
A	aspect ratio; measurements made to fuselage center line, b^2/S
A_e	effective aspect ratio, determined from experimental data
$(C_{L\alpha})_V$	lift-curve slope of vertical tail based on area of vertical tail per deg

$$C_{L\beta} = \frac{\partial C_L}{\partial \beta} \text{ per deg}$$

$$C_{n\beta} = \frac{\partial C_n}{\partial \beta} \text{ per deg}$$

$$C_{Y\beta} = \frac{\partial C_Y}{\partial \beta} \text{ per deg}$$

Subscripts:

W wing

F fuselage

V vertical tail
H horizontal tail

MODEL AND APPARATUS

Details of the model tested are shown in figure 2. The 45° swept wing and the fuselage of reference 1 were used in the present investigation. A new steel rear fuselage section was used with an aluminum-alloy vertical and horizontal tail. The wing and horizontal tail had a sweep angle of 45° at the quarter-chord line, an aspect ratio of 4, taper ratio of 0.6, and an NACA 65A006 airfoil section. The vertical tail was swept back 45° at the trailing edge, had an aspect ratio of 1.177, and had an NACA 63(10)A009 airfoil section.

The model was tested on the sting-support system shown in figure 3. With this support system the model can be remotely operated through a 28° angle-of-attack range in the plane of the vertical strut. The use of couplings in the sting behind the model makes it possible to support the model at angles of sideslip of -4° or 4° while the model is tested through the angle-of-attack range.

TESTS AND CORRECTIONS

The tests were conducted in the Langley high-speed 7- by 10-foot tunnel through a Mach number range from approximately 0.4 to 0.95. The size of the model caused the tunnel to choke at a Mach number of about 0.96. The blocking corrections, which were applied, were determined by the method of reference 2.

The jet-boundary corrections, which were applied to the angle of attack, were determined by the method of reference 3. The corrections to the lateral force, yawing moment, and rolling moment were investigated and were considered negligible.

No tare corrections, for the effect of the sting support, have been applied to the data. The results of an investigation to determine tares indicated that for the model without the vertical tail there were no tare forces present; however, with the addition of the vertical tail, small tare corrections to $C_{n\beta}$ and $C_{y\beta}$ were apparent at angles of attack above 8° . The data herein have not been corrected for these tares. However, if it is desired to apply these corrections an increment of $C_{n\beta}$ equal to -0.00025 and of $C_{y\beta}$ equal to 0.0005 should be

added to the data of the vertical-tail-on configurations above 8° angle of attack. The tare corrections to the effective-dihedral derivative C_{l_β} were negligible for all configurations tested.

During the actual running of the tests, difficulty was experienced with the lateral-force component of the strain-gage balance not maintaining a constant zero. Because of the erratic nature of this zero drift, it was not possible to correct the lateral-force data. The magnitude of the lateral-force derivative C_{Y_β} may be in error (generally low) by as much as 0.001; however, it is believed that the variations of C_{Y_β} with Mach number and angle of attack are fairly accurate representations of the correct variations.

The angle of attack and angle of sideslip have been corrected for the deflection of the sting-support system and balance under load. Corrections to rolling moment for the aeroelastic distortion of the wing have not been applied to the data. These corrections were evaluated, however, and were discussed in reference 1.

The variation of mean test Reynolds number with Mach number is presented in figure 4.

RESULTS AND DISCUSSION

Presentation of Results

The results of the investigation are presented in the following figures:

	Figure
Basic data C_{Y_β} , C_{n_β} , and C_{l_β} against α	5
Basic data C_{Y_β} , C_{n_β} , and C_{l_β} against M	6
Vertical-tail contributions	7 to 9
Center of pressure of load due to tail	10 and 11
Effective aspect ratio of vertical tail	12
Effect of Mach number on vertical-tail contribution	13
Wing interference increments on vertical-tail contributions	14

The wing-fuselage data and fuselage-alone data shown in figures 5 and 6 are the same data presented in reference 1 and are included here for completeness and for easy comparison with the other results.

The system for designating the various model configurations are defined as follows:

Complete model	WFBH
Wing, fuselage, and vertical tail	WFB
Wing and fuselage	WB
Fuselage, vertical tail, and horizontal tail	FHB
Fuselage and vertical tail	FB
Fuselage alone	B

Methods of Analysis

The results of the investigation are analyzed in terms of the wing-on and wing-off vertical-tail contributions. In the application of the wing-on results herein, it should be remembered that the model is a mid-wing configuration. The vertical-tail contributions were determined from the data by the following expressions:

For the wing-on condition

$$(C_{n\beta})_V = (C_{n\beta})_{WFB} - (C_{n\beta})_{WB} \quad (1)$$

and for the wing-off condition

$$(C_{n\beta})_V = (C_{n\beta})_{FHB} - (C_{n\beta})_B \quad (2)$$

The contributions $(C_{Y\beta})_V$ and $(C_{l\beta})_V$ were determined in a like manner and these increments are presented in figure 7.

The contribution of the vertical tail can also be expressed by the following equations:

$$(C_{Y\beta})_V = - (C_{L\alpha})_V \frac{S_Y}{S_W} \eta_Y \quad (3)$$

$$(C_{n\beta})_V = (C_{L\alpha})_V \frac{z_V}{b_W} \frac{S_Y}{S_W} \eta_n \quad (4)$$

$$(C_{l\beta})_V = (C_{l\alpha})_V \frac{S_V}{S_W} \left(\frac{l_V}{b_W} \sin \alpha - \frac{z_V}{b_W} \cos \alpha \right) \quad (5)$$

where $(C_{l\alpha})_V$ is the effective lift-curve slope of the vertical tail at zero angle of attack and η_Y and η_n are correction factors which account for the variation in tail effectiveness with angle of attack. These correction factors were derived from the data and are presented in figure 9. The effective aspect ratio $(A_e)_V$, corresponding to the effective lift-curve slope $(C_{l\alpha})_V$ determined from experimental values of $C_{n\beta}$ by equations (2) and (4), is presented in figure 12(a). These effective aspect ratios $(A_e)_V$ were evaluated by using the theory of reference 4 with compressibility effects accounted for by the theory of reference 5.

The effective tail lengths l_V and tail heights z_V were derived using experimental data and equations (4) and (5) and are presented in figures 10 and 11.

The rate of change with angle of attack of the effective-dihedral derivative contributed by the vertical tail $\frac{\partial (C_{l\beta})_V}{\partial \alpha}$ is shown in figure 8 and was calculated, for small angles of attack, by the following expression:

$$\frac{\partial (C_{l\beta})_V}{\partial \alpha} = \frac{(C_{l\alpha})_V}{57.3} \frac{l_V}{b_W} \frac{S_V}{S_W} \quad (6)$$

where $(C_{l\alpha})_V$ was obtained from reference 4 by using an effective aspect ratio determined by applying the fuselage end-plate effect from the faired values of reference 6 to the geometric aspect ratio of the vertical tail. Compressibility effects were accounted for by the method of reference 5. The center of load used in the calculations was assumed to be at the $\bar{c}_V/4$ of the vertical tail. An examination of the change in $(C_{l\alpha})_V$ due to the change in the effective plan form of the vertical tail with an increase in angle of attack indicated that the effect on

$\frac{\partial (C_{l\beta})_V}{\partial \alpha}$ was negligible. Therefore, in the differentiation of equation (5), in order to obtain equation (6), $(C_{L\alpha})_V$ was held constant.

The interference of the wing on the vertical-tail effectiveness for both the horizontal-tail-on and horizontal-tail-off conditions are presented in figure 14 and were determined (by using notations used in ref. 6 for consistency) as follows:

For the horizontal-tail-on condition

$$\Delta_2 C_{n\beta} = \left[(C_{n\beta})_{WFVH} - (C_{n\beta})_{WF} \right] - \left[(C_{n\beta})_{FVH} - (C_{n\beta})_F \right]$$

and for the horizontal-tail-off condition

$$\Delta_2 C_{n\beta} = \left[(C_{n\beta})_{WFFV} - (C_{n\beta})_{WFF} \right] - \left[(C_{n\beta})_{FFV} - (C_{n\beta})_F \right]$$

The increments $\Delta_2 C_{Y\beta}$ and $\Delta_2 C_{l\beta}$ were determined in a like manner.

Vertical-Tail Contributions

Effect of angle of attack.- The directional-stability results presented in figures 7 and 9 indicate a large reduction in vertical-tail effectiveness at the higher angles of attack. Even though this reduction in η_n is quite large (fig. 9), the data of figure 7 indicate that the vertical tail contributes a stabilizing increment at all angles of attack. A comparison of the data of figure 9 with the faired curve from figure 23(b) of reference 6 shows that the data herein indicate a more rapid reduction at the higher angles. This reduction may be due to the difference in fuselage shape. It should be noted that fuselage 5 of reference 6, which is similar to the fuselage used herein, also indicates a much greater decrease than the faired curve (fig. 24(a) of ref. 6).

The dihedral effect contributed by the vertical tail is seen to decrease with angle of attack in the usual manner (fig. 7(c)). The

variation of the slope $\frac{\partial (C_{l\beta})_V}{\partial \alpha}$ with Mach number is presented in figure 8 along with calculated values. The measured slopes are seen to be considerably greater than the calculated values.

Effective tail lengths.- The locations of the center of load of the vertical tail were determined by the use of equations (3), (4), and (5) (letting η_Y and η_n equal 1.0) and are presented in figures 10 and 11. As previously mentioned, the lateral-force derivative $C_{Y\beta}$ probably is slightly in error and therefore the actual location of the center of load is probably somewhat forward of and below the location indicated. However, this error in $C_{Y\beta}$ is not expected to greatly affect the variation of the center of load with Mach number and angle of attack. The results of figure 10 indicate that there is essentially no effect of Mach number on the center-of-load location at zero angle of attack. For the wing-on condition (fig. 11) the center of load is seen to move down with an increase in angle of attack and the rate of this downward movement with angle of attack increases with Mach number. For the wing-off condition, there was a rapid forward movement of the center of load at the highest angle of attack.

Effective aspect ratio.- The variation with Mach number of the effects of the fuselage and horizontal tail on the effective aspect ratio of the vertical tail at zero angle of attack is presented in figure 12. The effective aspect ratio of the vertical tail was obtained by calculating the tail lift-curve slope from the experimental values of $(C_{n\beta})_V$ by use of equation (4) where the geometric tail lengths were applied, and then by obtaining the corresponding aspect ratio from the theory for plain wings. The theory of reference 4 was used for determining the three-dimensional incompressible-flow values of $(C_{l\alpha})_V$ with the effect of compressibility accounted for by the method of reference 5.

The results presented in figure 12(a) show a decrease in the end-plate effect of the fuselage with Mach number. If the scatter of the data of reference 6 is considered, the comparison with the present data is quite good.

The horizontal tail, in the position used for these tests, shows very little effect on the lateral-stability coefficients (fig. 5) or on the effective aspect ratio of the vertical tail (fig. 12(b)). This is in agreement with the results of reference 7.

Prediction of tail contributions.- Some predictions of the tail contributions to the lateral-stability derivatives throughout the Mach number

range are presented in figure 13 along with the experimental results. The calculated contributions, evaluated by applying the fuselage end-plate effect from reference 6 to the geometric aspect ratio for determining $(C_{l_\alpha})_V$ from reference 4, show good agreement with the experimental results. The geometric center of pressure $\bar{c}_V/4$ was used in the calculations.

Wing interference on tail effectiveness.- The interference of the wing on the contribution of the vertical tail is presented in figure 14 for two Mach numbers. At the lower angles of attack, the effect of the wing is small compared with the direct contribution of the vertical tail. At the higher angles of attack (from $\alpha = 12^\circ$ to $\alpha = 23^\circ$) wing interference produces a destabilizing increment to the directional stability derivative $(C_{n_\beta})_V$ for the horizontal-tail-off configuration (fig. 14(a)). For the horizontal-tail-on configuration at these angles of attack, wing interference contributes a stabilizing increment to $(C_{n_\beta})_V$ (fig. 14(b)). The effects of Mach number are small and inconclusive. Comparison with the wing-interference data of reference 6 indicates reasonably good agreement.

CONCLUSIONS

The results of the investigation to determine the effect of the vertical and horizontal tails on the lateral stability of a general research model up to a Mach number of 0.95 indicated that, in general, Mach number effects and wing effects were small and the overall trends of the data of the present investigation agreed with those which have been established from low-speed investigations. The following specific conclusions are indicated for the midwing model investigated.

1. The contribution of the vertical tail to the directional stability $(C_{n_\beta})_V$ at zero angle of attack increases slightly with Mach number and can be predicted with satisfactory accuracy when the load is assumed to act as the aerodynamic center of the vertical tail $\bar{c}_V/4$ and when the end-plate effect of the fuselage on the theoretical lift-curve slope of the tail is considered. The vertical tail contributes a stabilizing increment at all angles of attack; however, at the higher angles this stabilizing increment is greatly reduced.

2. The contribution of the vertical tail to the effective dihedral derivative C_{l_β} at zero angle of attack increases slightly with Mach number and can be satisfactorily estimated when the geometric center of load $\bar{c}_V/4$ and the end-plate effect of the fuselage on the theoretical

lift-curve slope of the tail are considered. The rate of change of the effective dihedral with angle of attack $\frac{\partial (C_{L\beta})_V}{\partial \alpha}$ was greater throughout the Mach number range than calculations indicated.

3. The end-plate effect of the fuselage on the vertical tail decreased with Mach number and indicated good agreement with low-speed data.

4. The interference effects of the wing and horizontal tail on the lateral-stability derivatives were small at the lower angles of attack.

Langley Aeronautical Laboratory,
National Advisory Committee for Aeronautics,
Langley Field, Va., May 20, 1953.

REFERENCES

1. Kuhn, Richard E., and Wiggins, James W.: Wind-Tunnel Investigation of the Aerodynamic Characteristics in Pitch of Wing-Fuselage Combinations at High Subsonic Speeds - Aspect-Ratio Series. NACA RM L52A29, 1952.
2. Hensel, Rudolph W.: Rectangular-Wind-Tunnel Blocking Corrections Using the Velocity-Ratio Method. NACA TN 2372, 1951.
3. Gillis, Clarence L., Polhamus, Edward C., and Gray, Joseph L., Jr.: Charts for Determining Jet-Boundary Corrections for Complete Models in 7- by 10-Foot Closed Rectangular Wind Tunnels. NACA WR L-123, 1945. (Formerly NACA ARR L5G31.)
4. DeYoung, John, and Harper, Charles W.: Theoretical Symmetric Span Loading at Subsonic Speeds for Wings Having Arbitrary Plan Form. NACA Rep. 921, 1948.
5. Fisher, Lewis R.: Approximate Corrections for the Effects of Compressibility on the Subsonic Stability Derivatives of Swept Wings. NACA TN 1854, 1949.
6. Queijo, M. J., and Wolhart, Walter D.: Experimental Investigation of the Effect of Vertical-Tail Size and Length and of Fuselage Shape and Length on the Static Lateral Stability Characteristics of a Model With 45° Sweptback Wing and Tail Surfaces. NACA Rep. 1049, 1951. (Supersedes NACA TN 2168.)
7. Brewer, Jack D., and Lichtenstein, Jacob H.: Effect of Horizontal Tail on Low-Speed Static Lateral Stability Characteristics of a Model Having 45° Sweptback Wing and Tail Surfaces. NACA TN 2010, 1950.

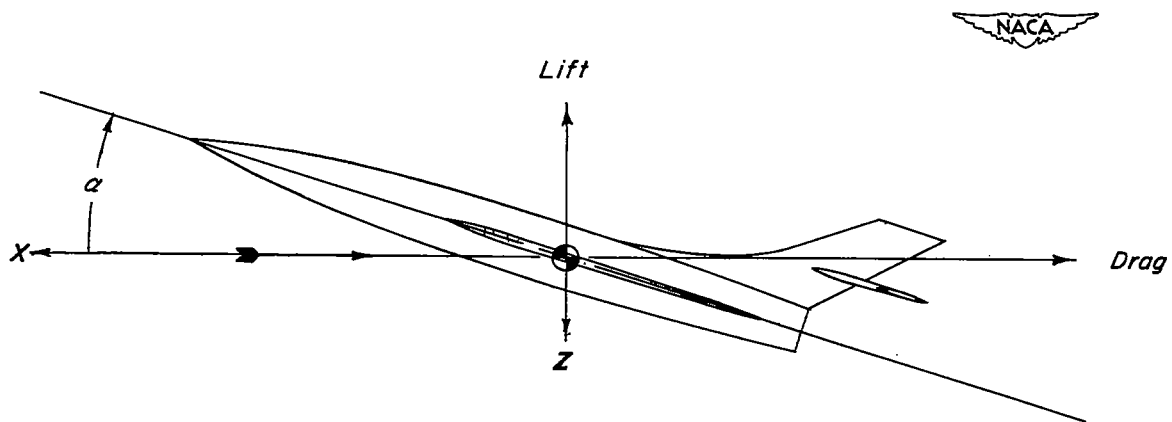
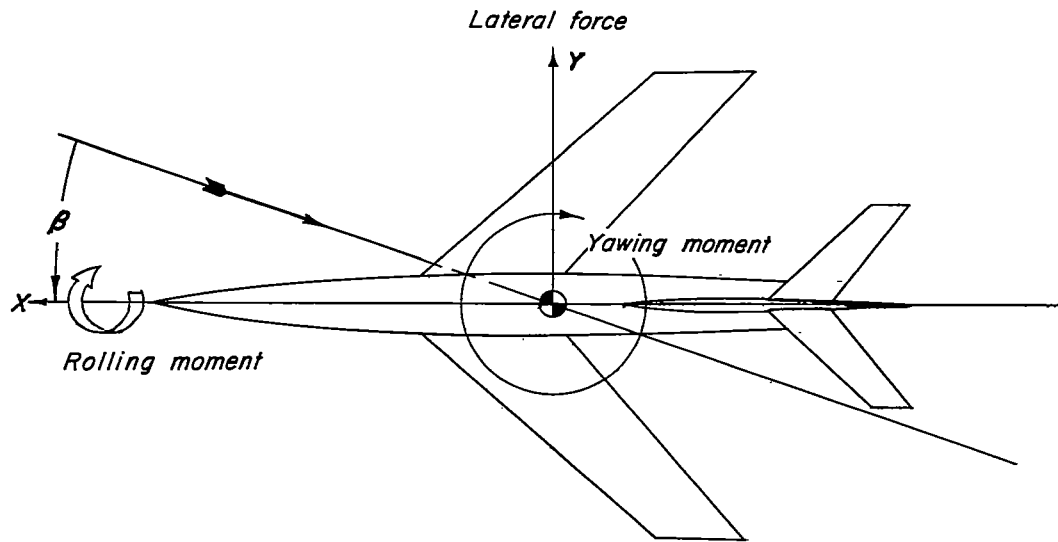
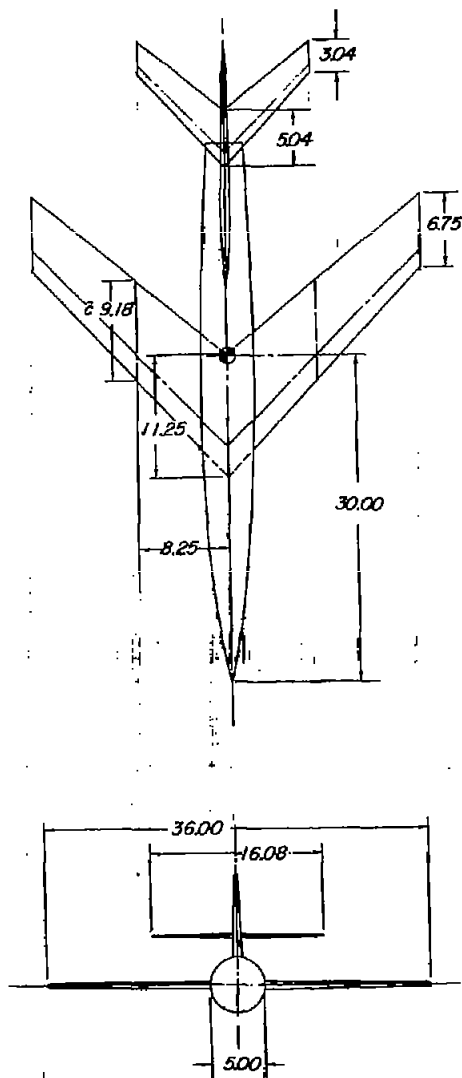


Figure 1.- System of axes used showing the positive direction of forces, moments, angles, and velocities.



<i>Wing</i>	
Area, sq ft	2.25
Aspect ratio	4
Sweep (b) $9/4$	45°
Taper ratio	.6
Airfoil section streamwise	NACA 65A006
<i>Horizontal tail</i>	
Area, sq ft	.45
Aspect ratio	4
Sweep (b) $9/4$	45°
Taper ratio	.6
Airfoil section streamwise	NACA 65A006
<i>Vertical tail</i>	
Area, sq ft	.612
Aspect ratio	1.177
Sweep (b) T.E.	45°
Taper ratio	.5
Airfoil section streamwise	NACA 63 _{nat} A009

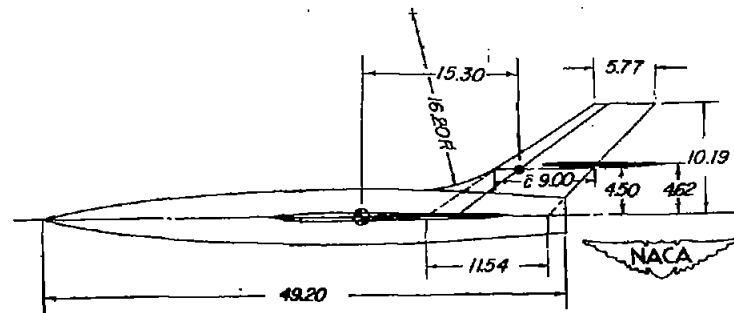


Figure 2.- Three-view drawing of model. All dimensions are in inches.

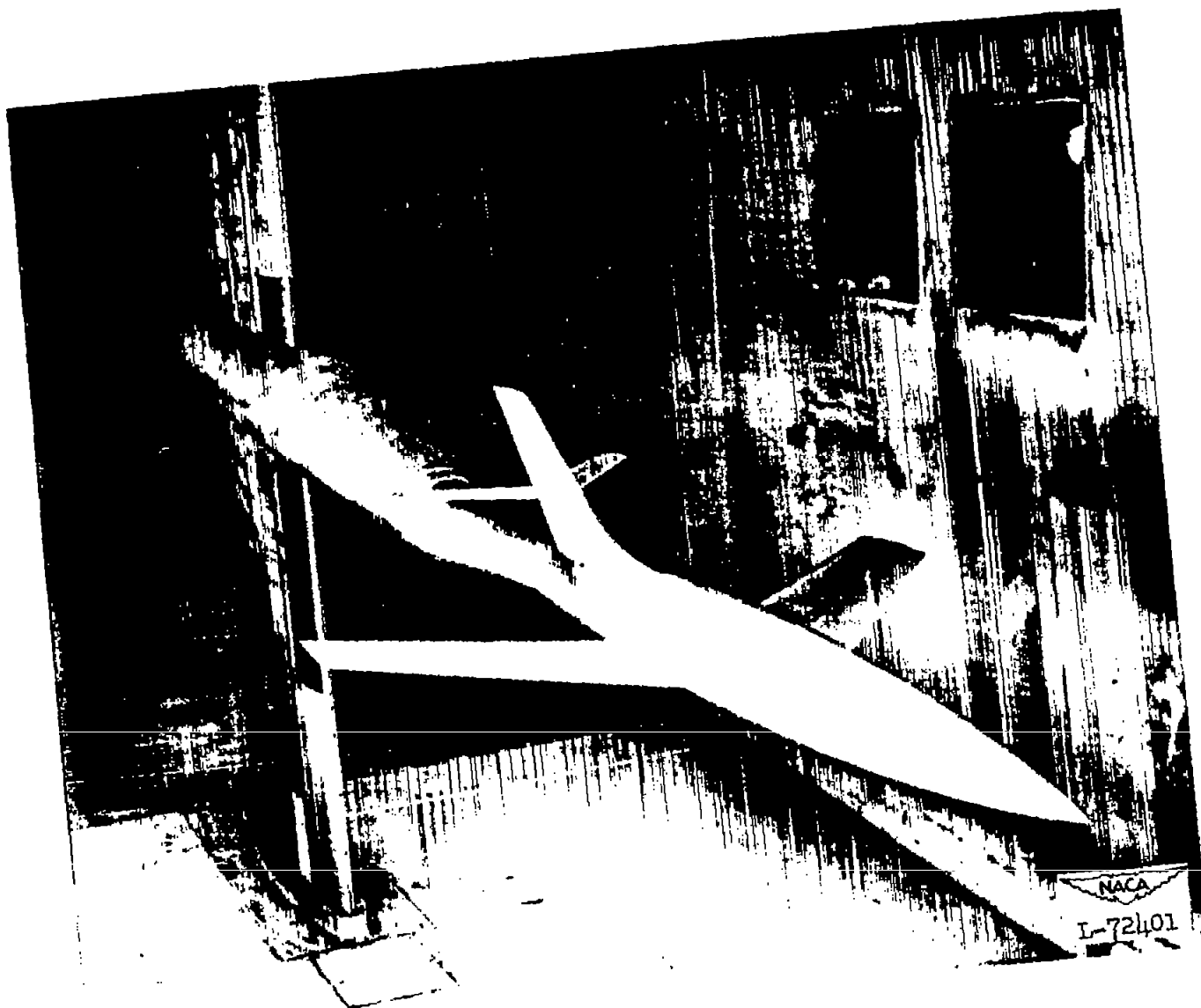


Figure 3.- Model on sting-support system.

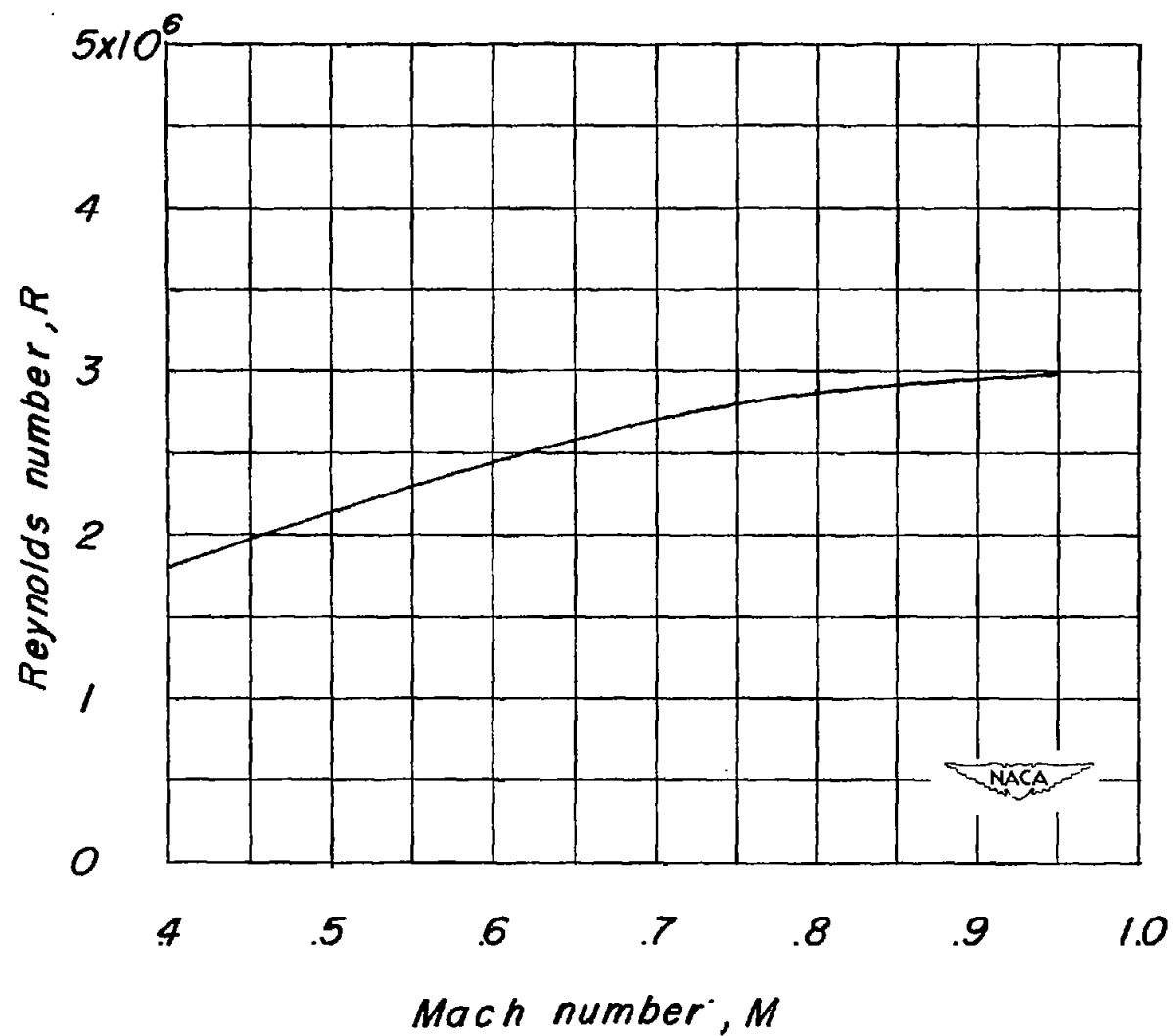


Figure 4.- Variation of mean test Reynolds number with test Mach number based on the wing mean aerodynamic chord of 0.765 foot.

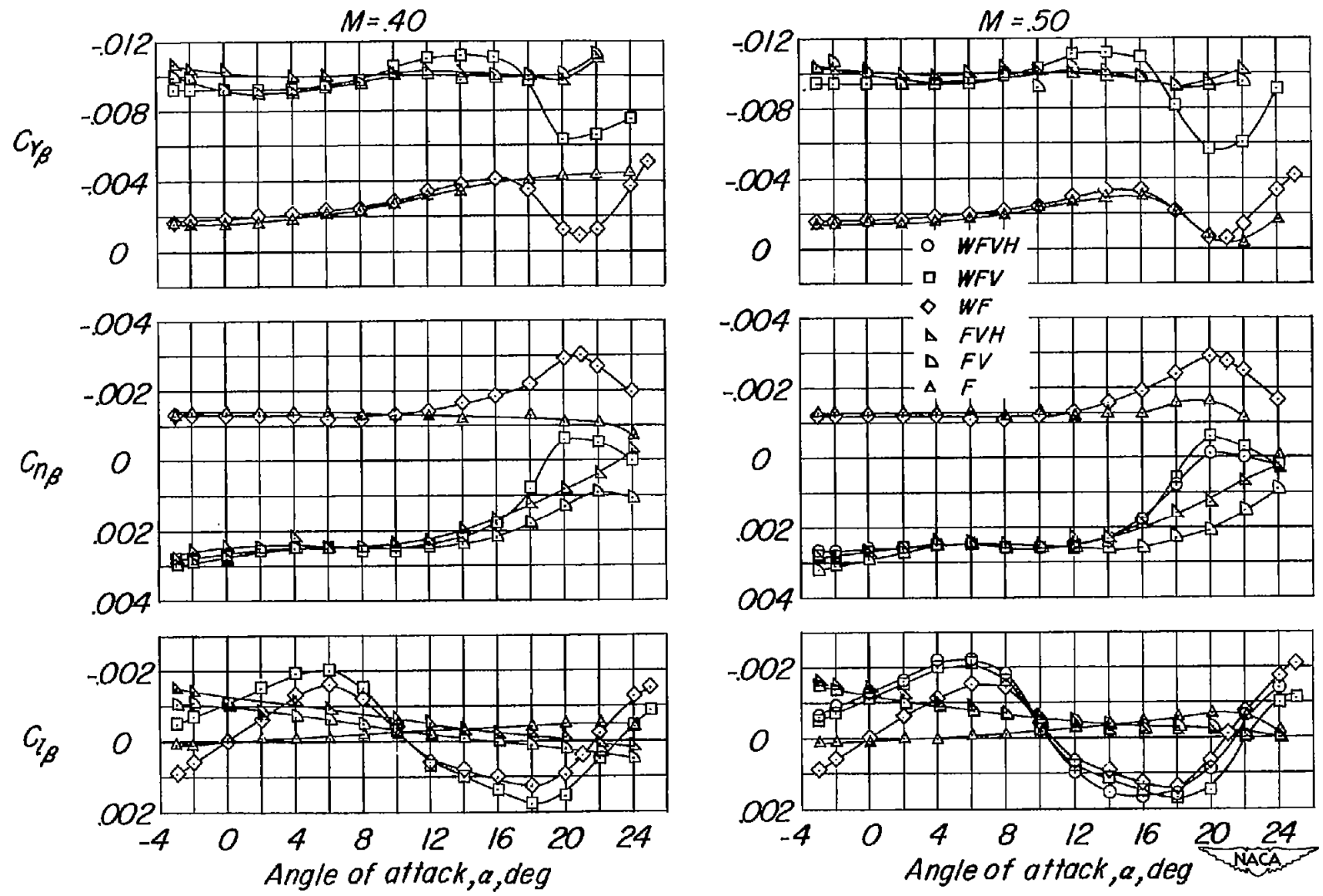


Figure 5.- Lateral stability characteristics of the various model configurations.

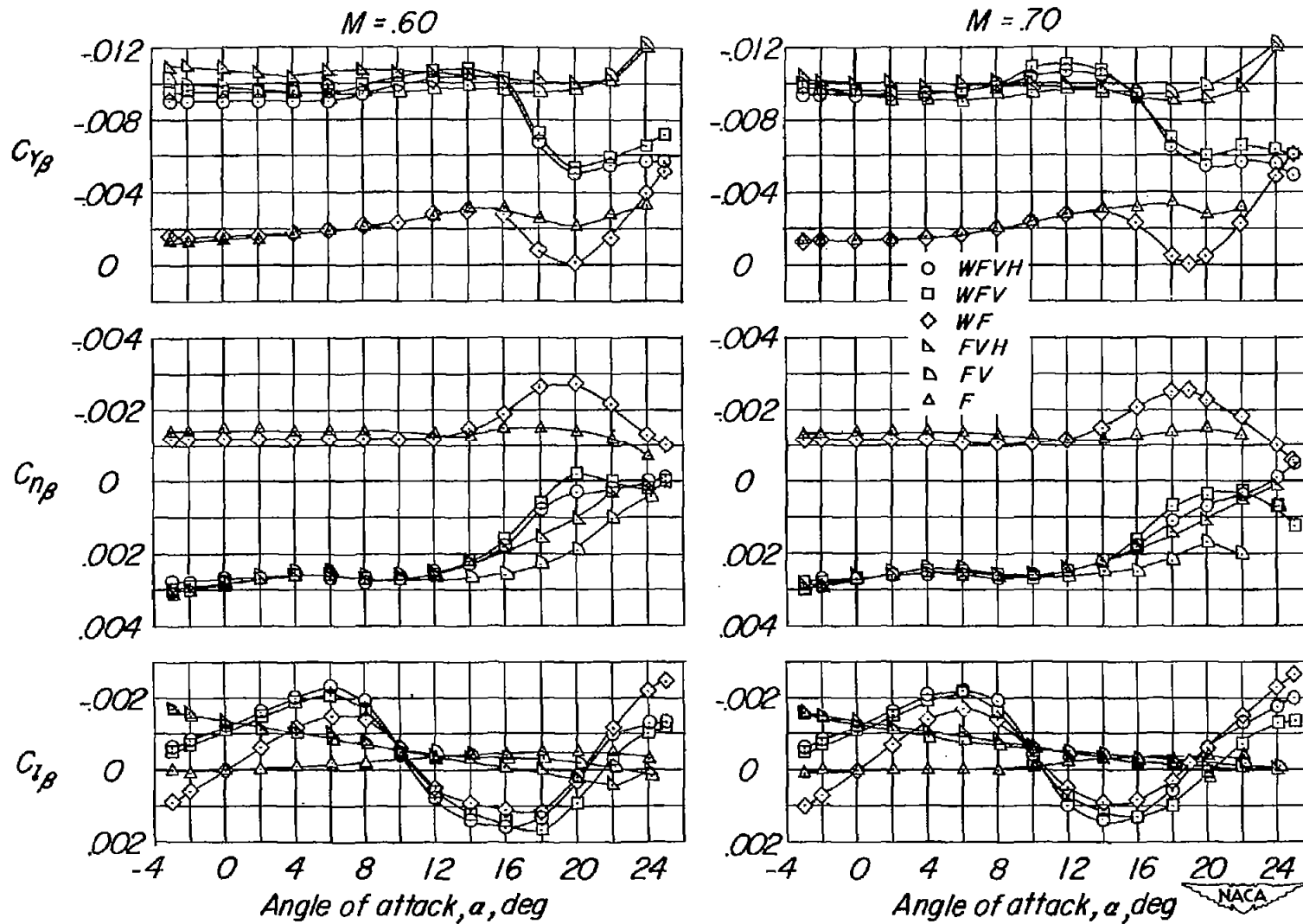


Figure 5.- Continued.

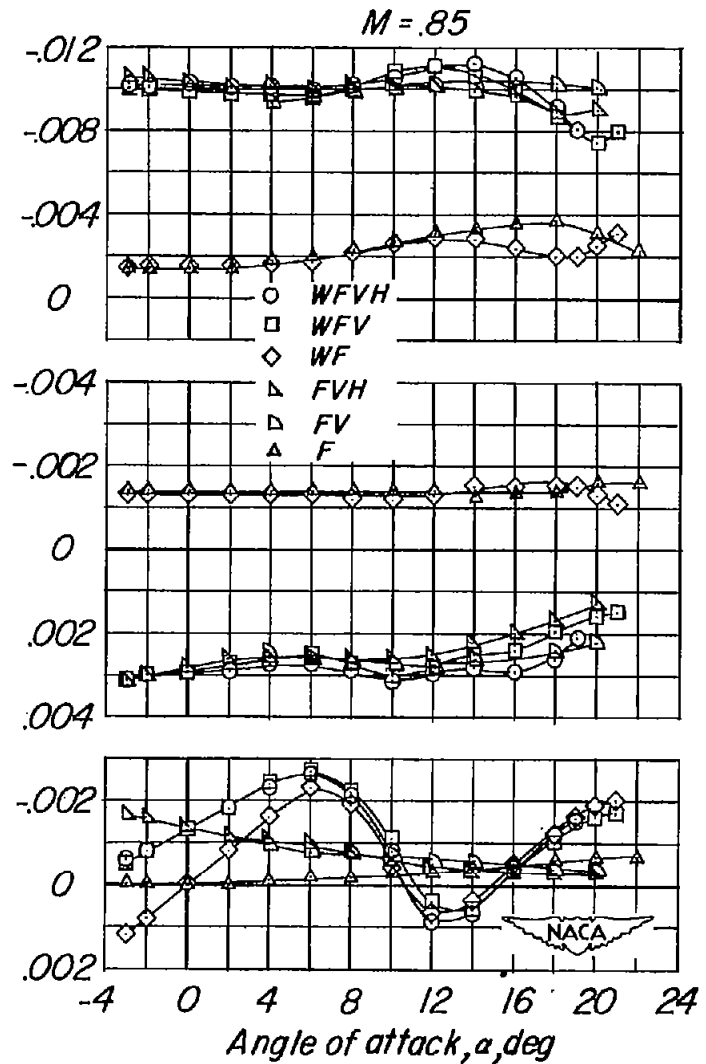
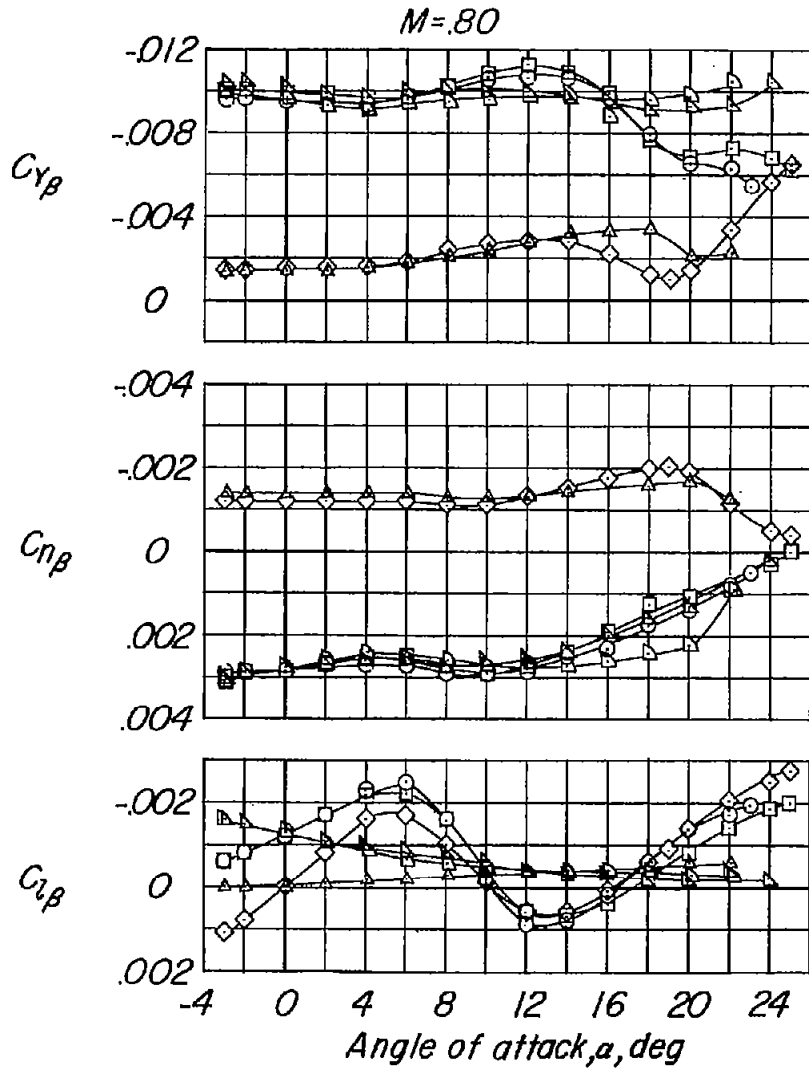


Figure 5.- Continued.

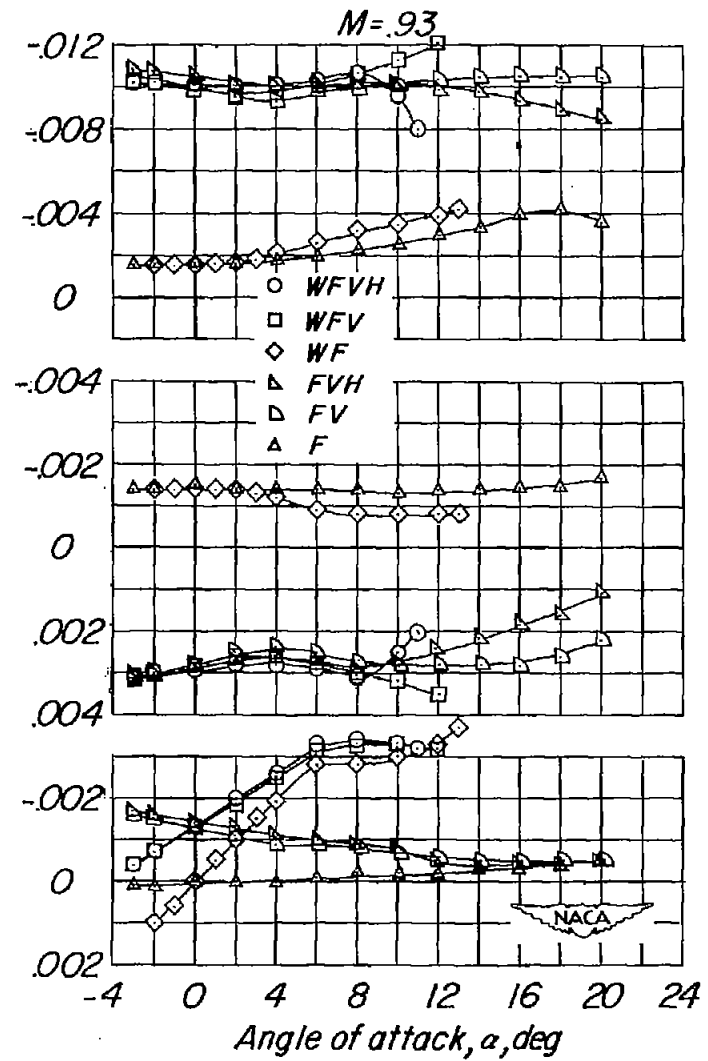
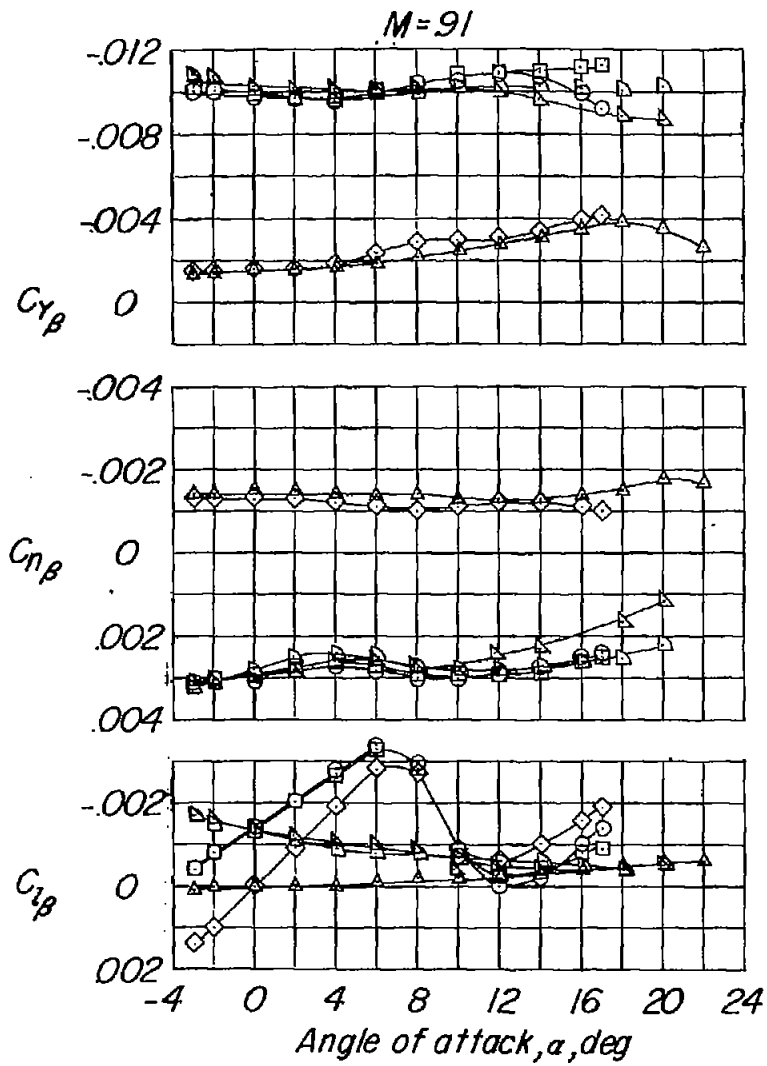


Figure 5.- Continued.

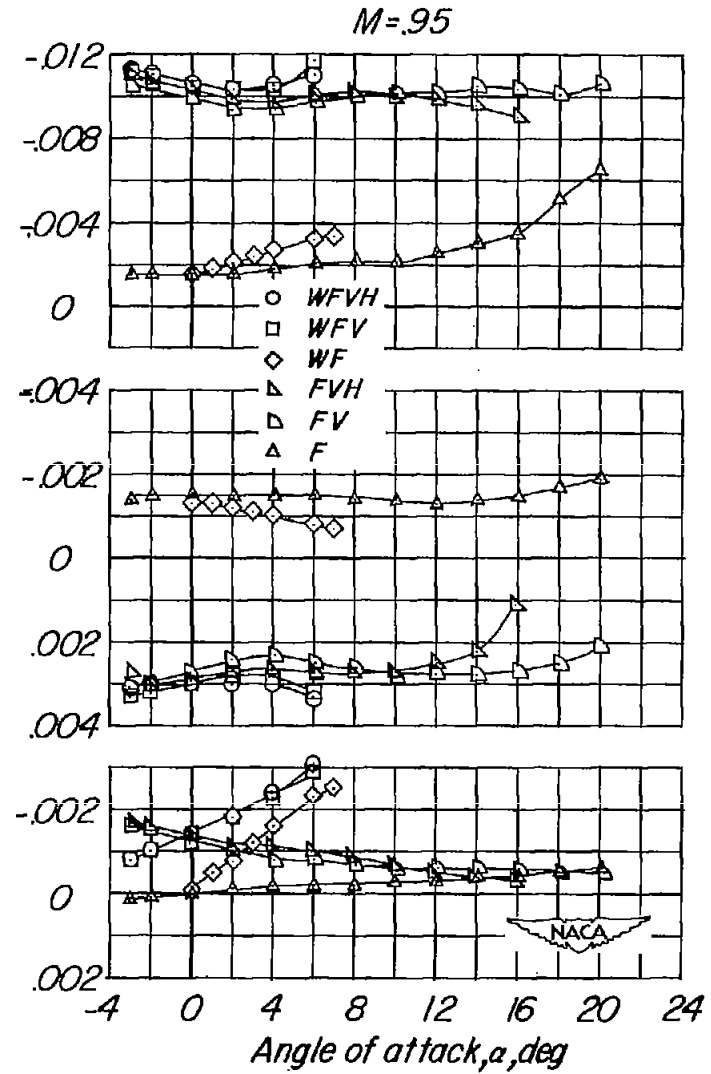
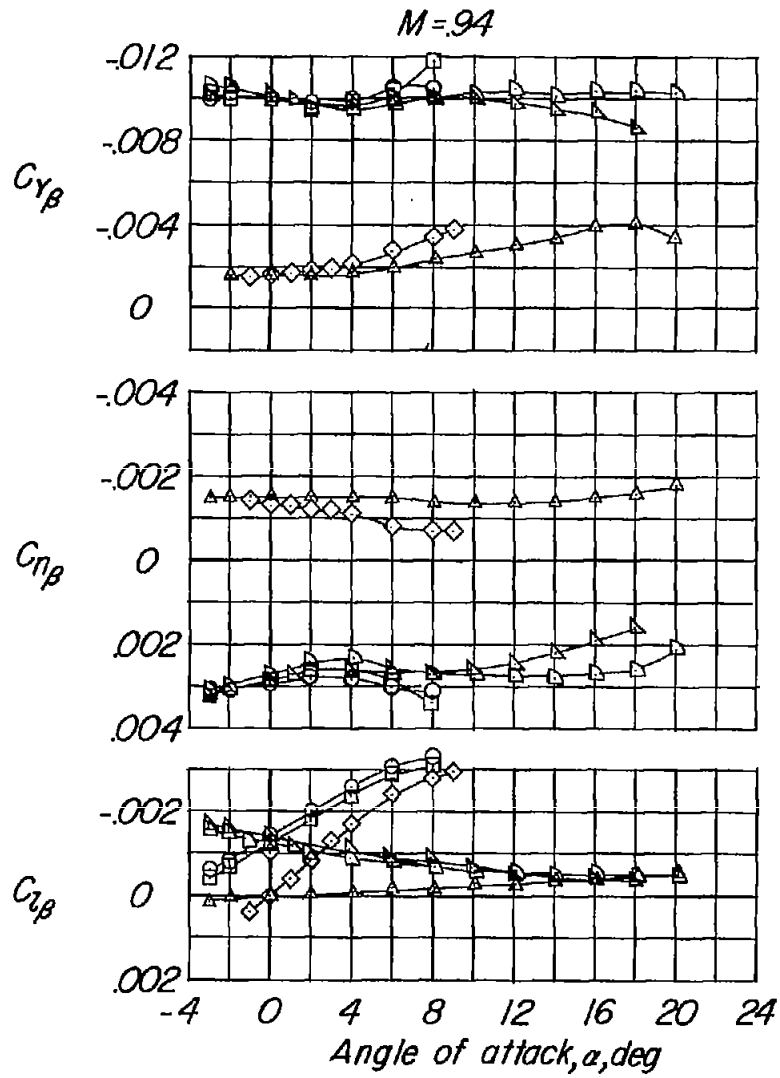


Figure 5.- Concluded.

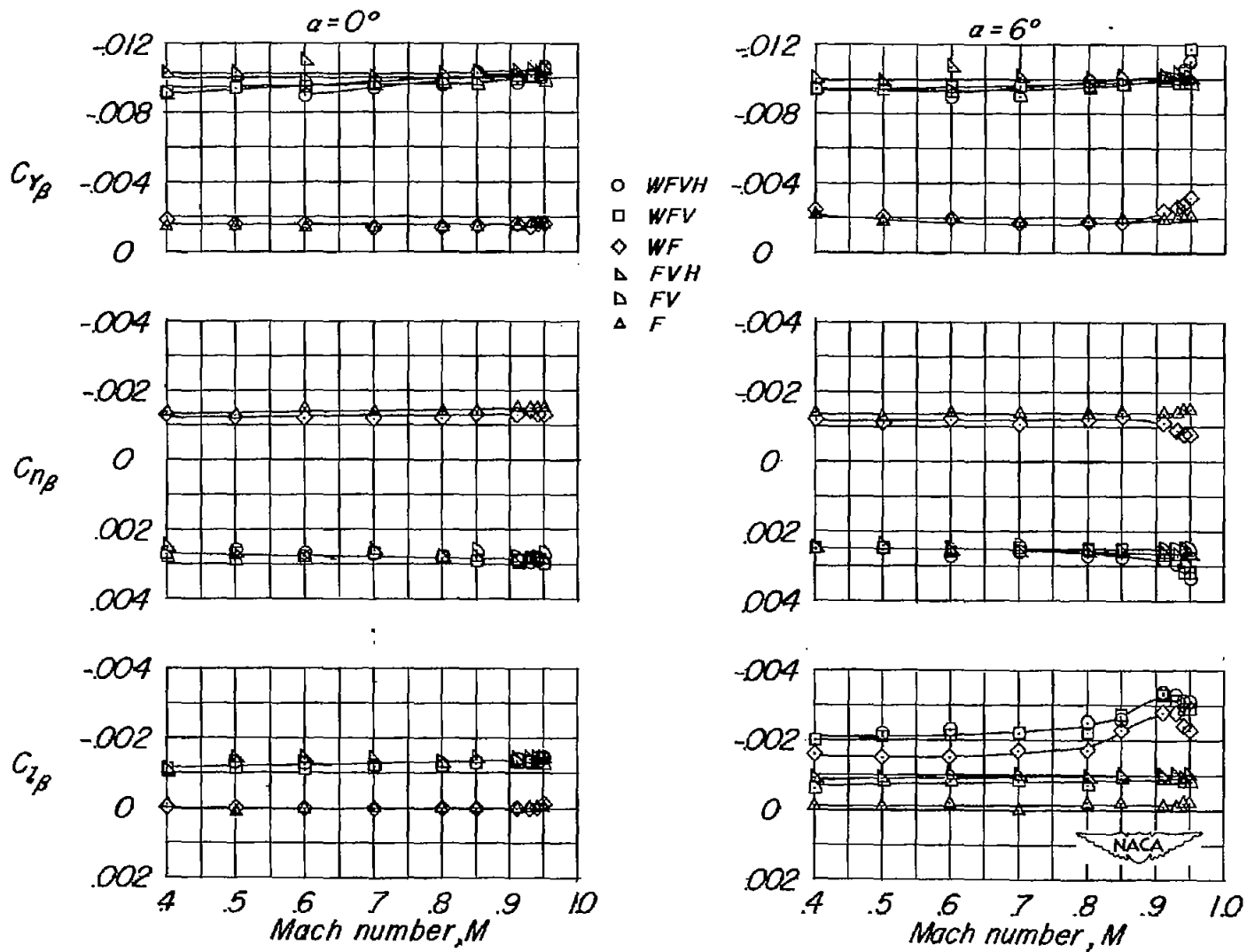


Figure 6.- Lateral stability characteristics of various model configurations through the Mach number range.

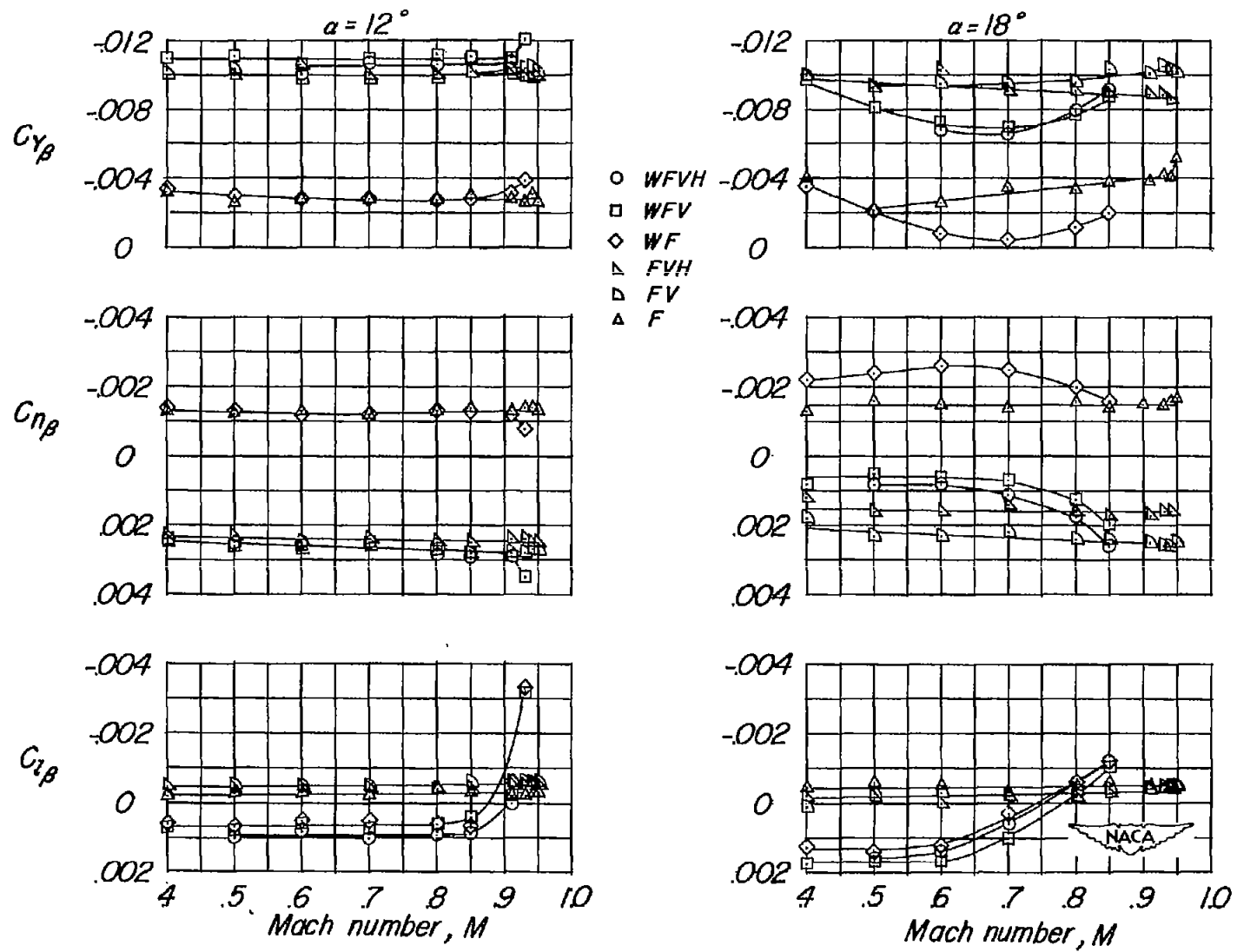


Figure 6.- Concluded.

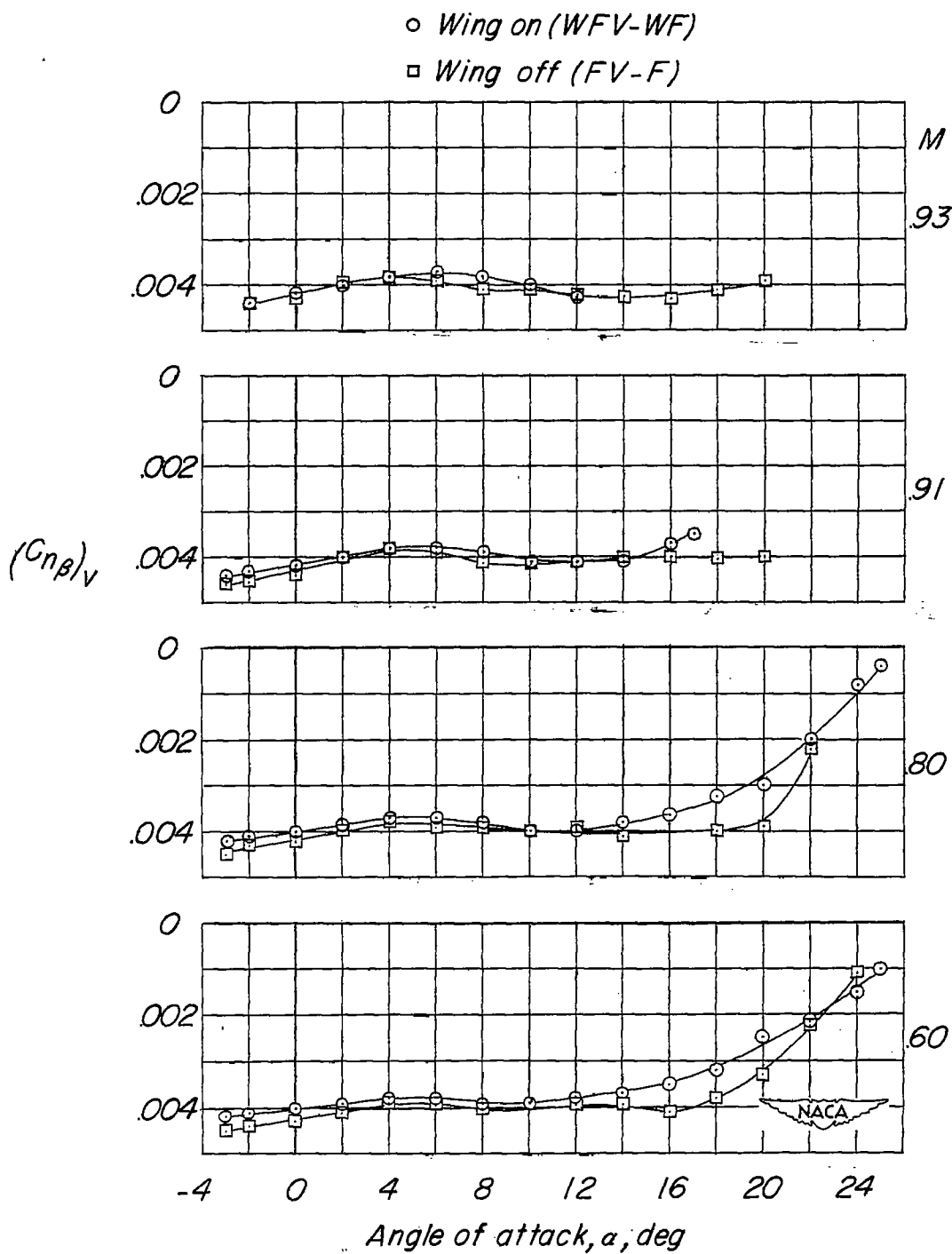


Figure 7.- Vertical-tail contribution to the directional-stability derivative, lateral-force derivative, and effective-dihedral derivative.

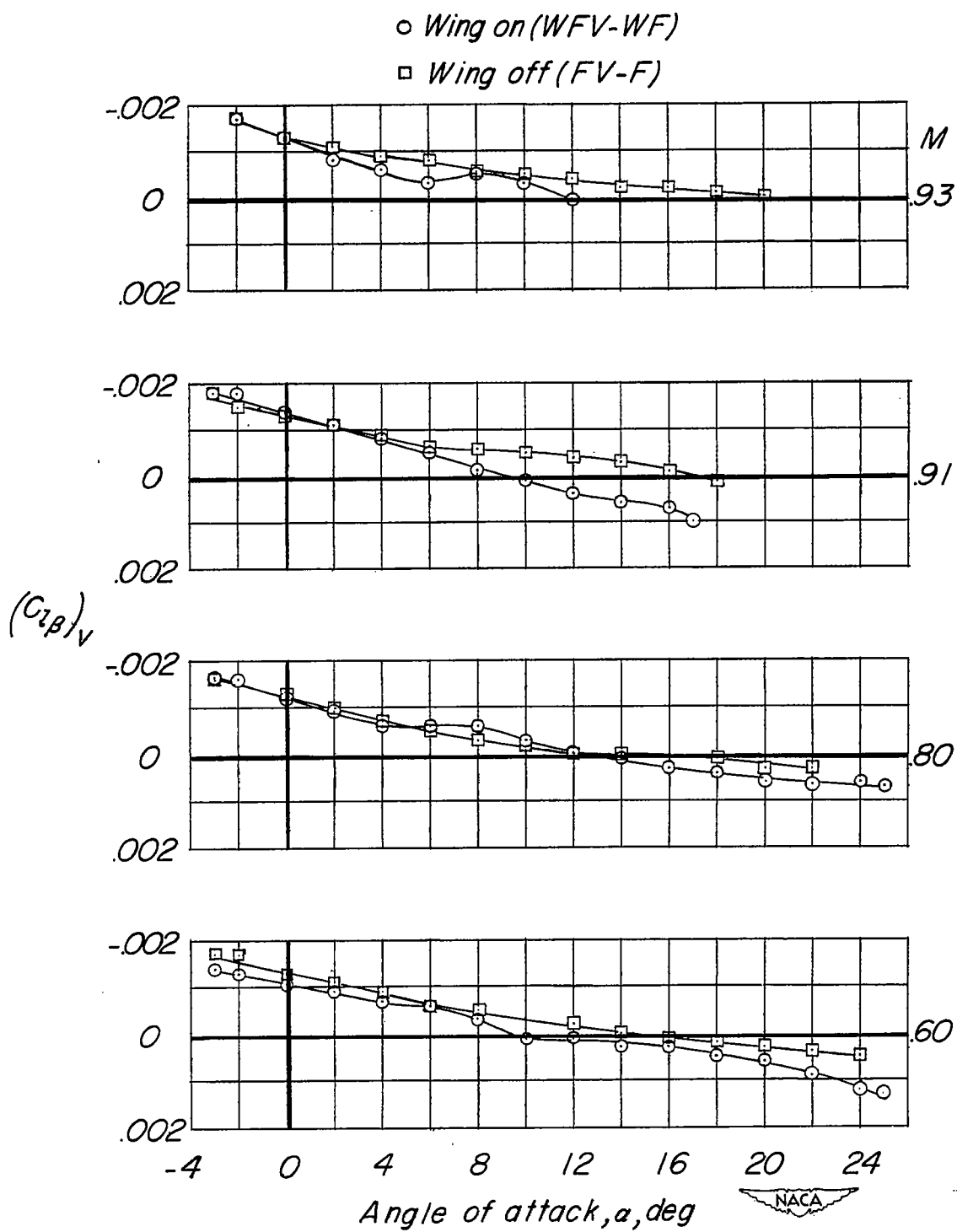
(c) C_{L_N} .

Figure 7.- Concluded.

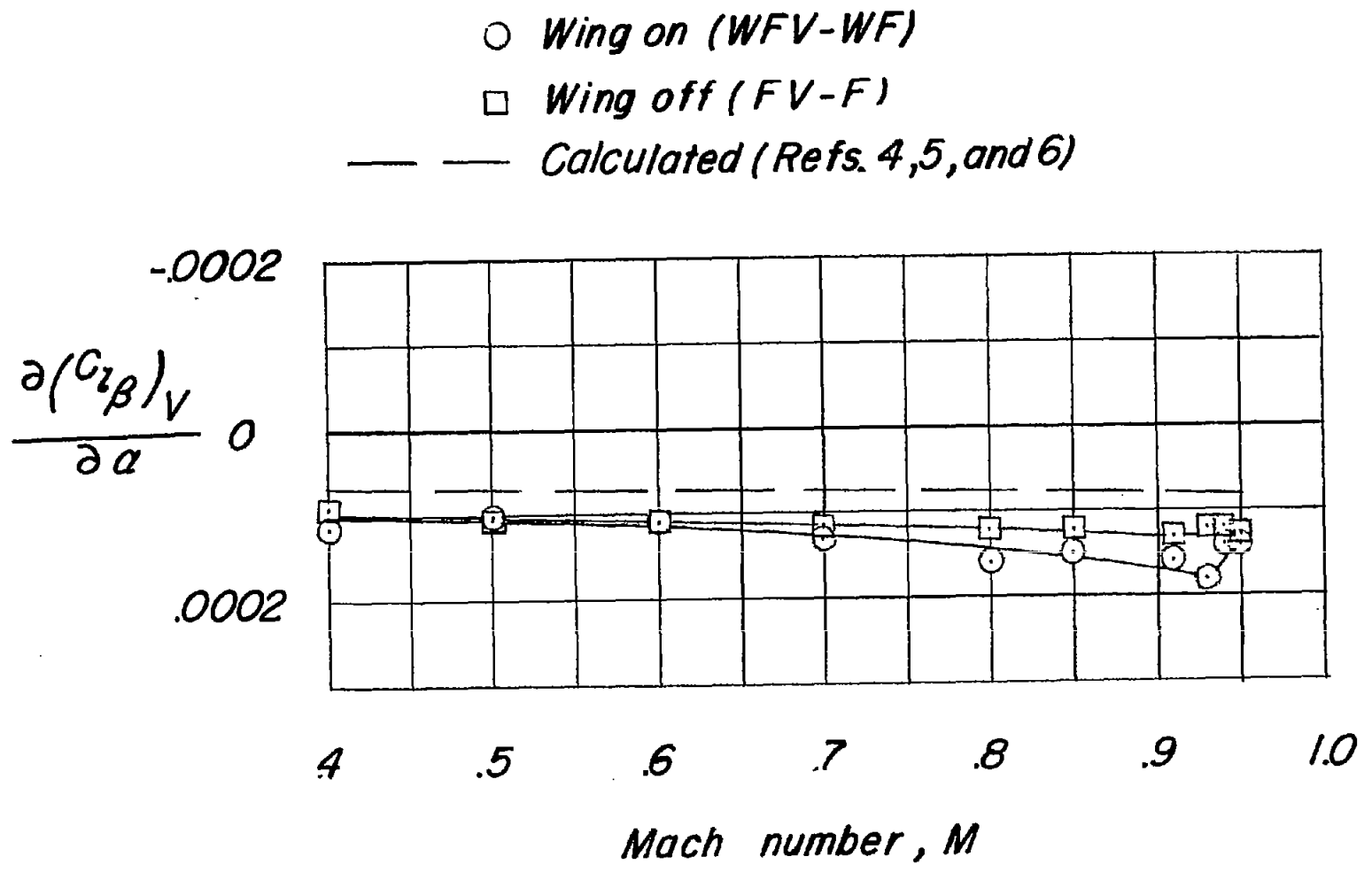


Figure 8.- The rate of change of the effective-dihedral derivative with angle of attack through the Mach number range.

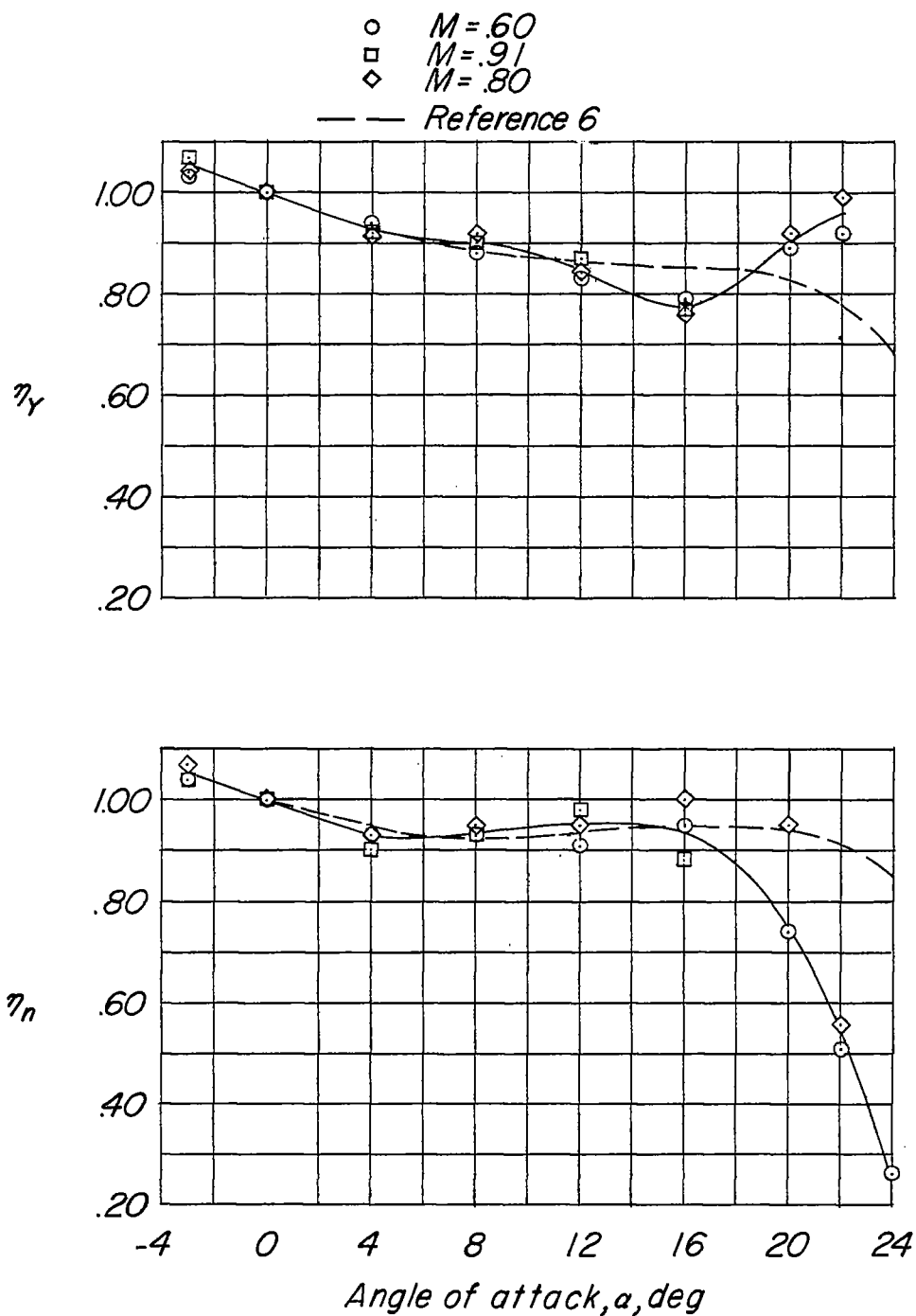


Figure 9.- The angle-of-attack correction factors to the vertical-tail contribution to $C_{n\beta}$ and $C_{Y\beta}$.

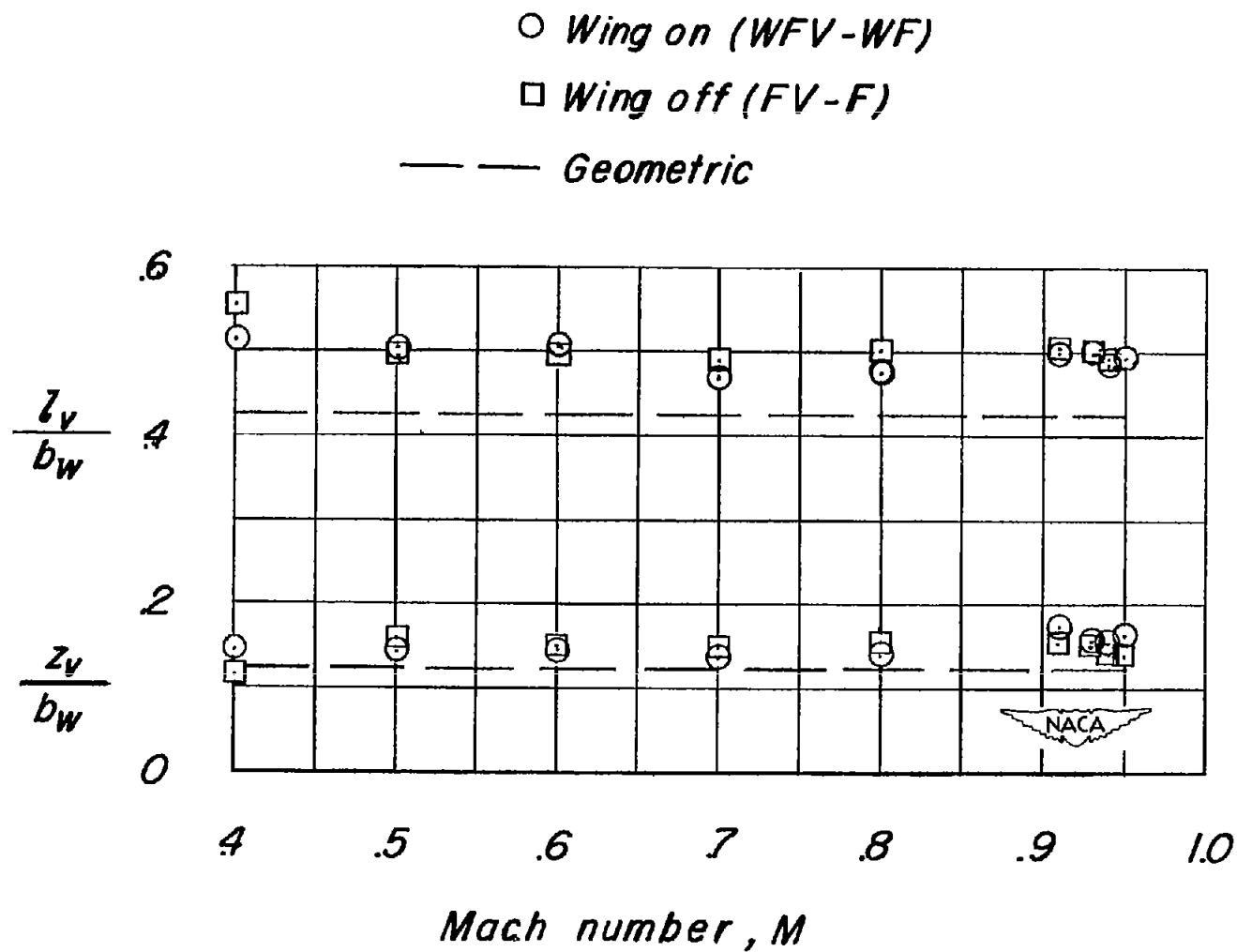


Figure 10.- Comparison of the experimentally determined center-of-pressure location with the geometric center of load through the Mach number range. $\alpha = 0^\circ$.

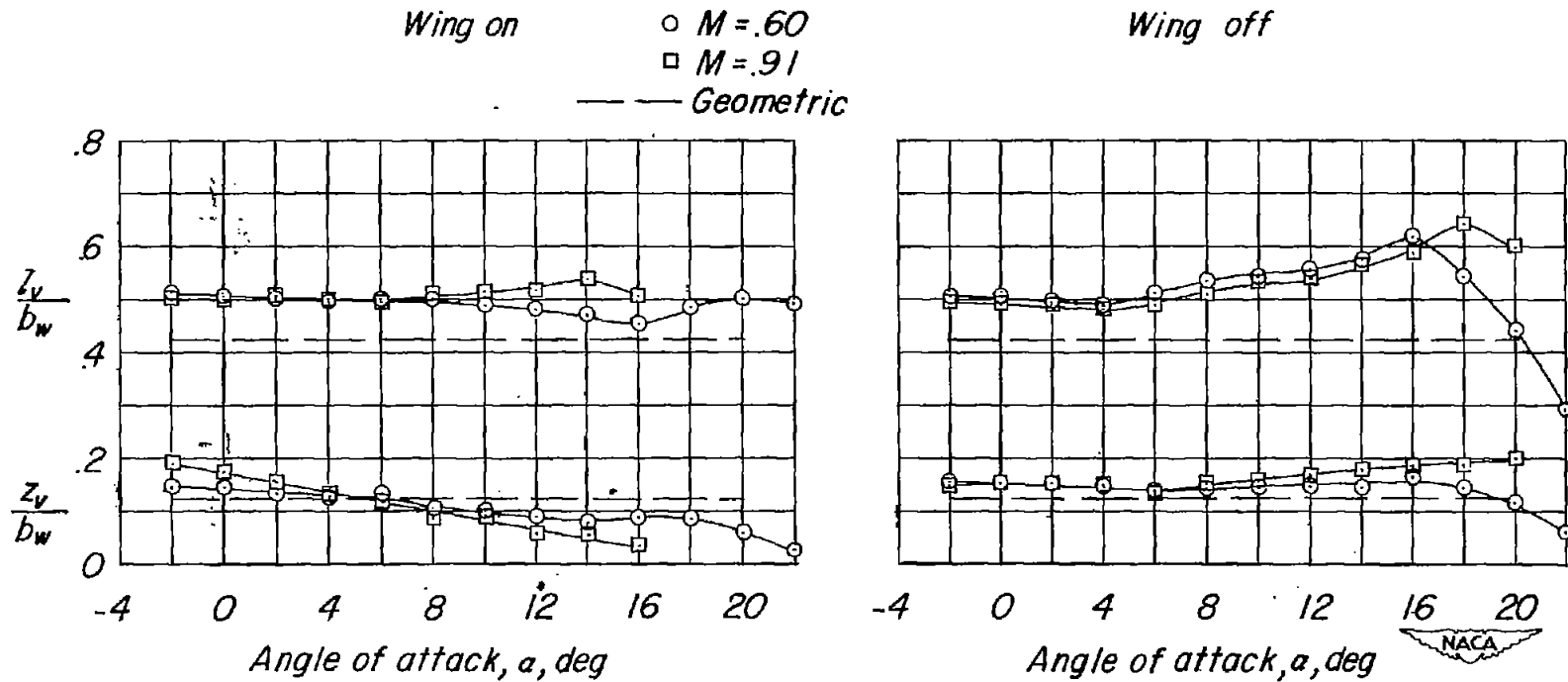
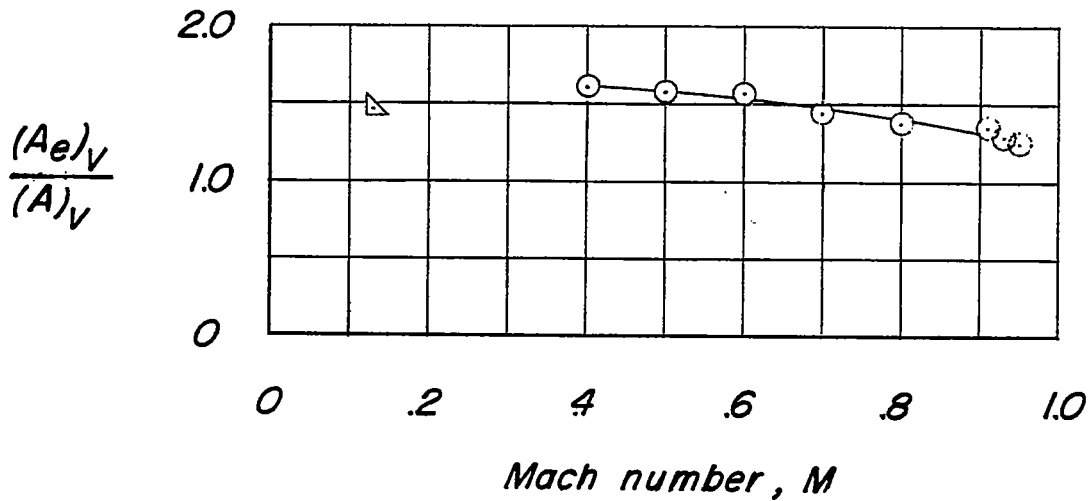
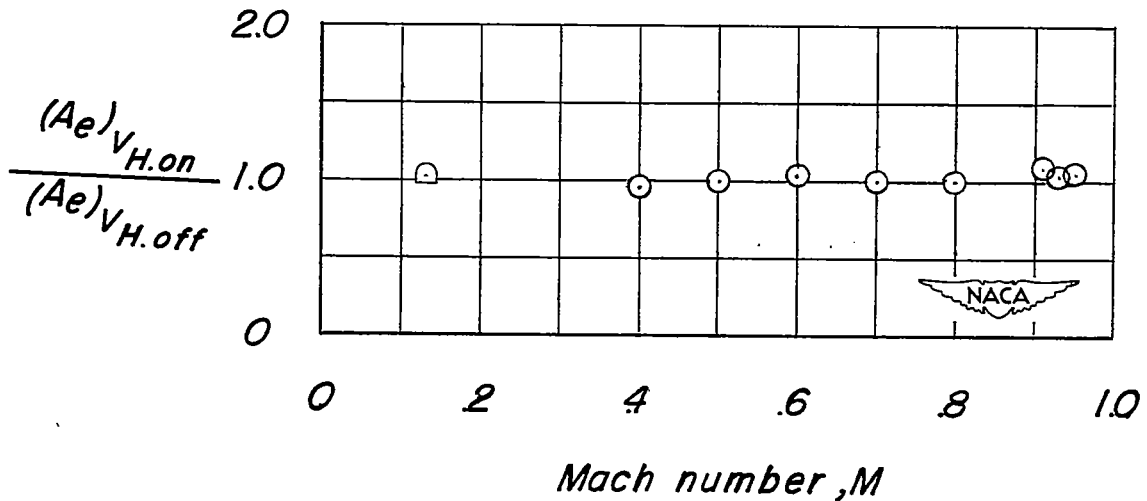


Figure 11.- Effect of angle of attack on the experimentally determined center-of-pressure location at Mach numbers of 0.60 and 0.91.

- *Exp. $C_{\eta\beta}$, geometric c.p.*
- △ *Faired curve of Ref. 6*
- ◻ *Ref. 7*



(a) Fuselage effect. Wing and horizontal tail off.



(b) Horizontal-tail effect. Wing off.

Figure 12.- Fuselage effect and horizontal-tail effect on the effective aspect ratio of the vertical tail. $\alpha = 0^\circ$.

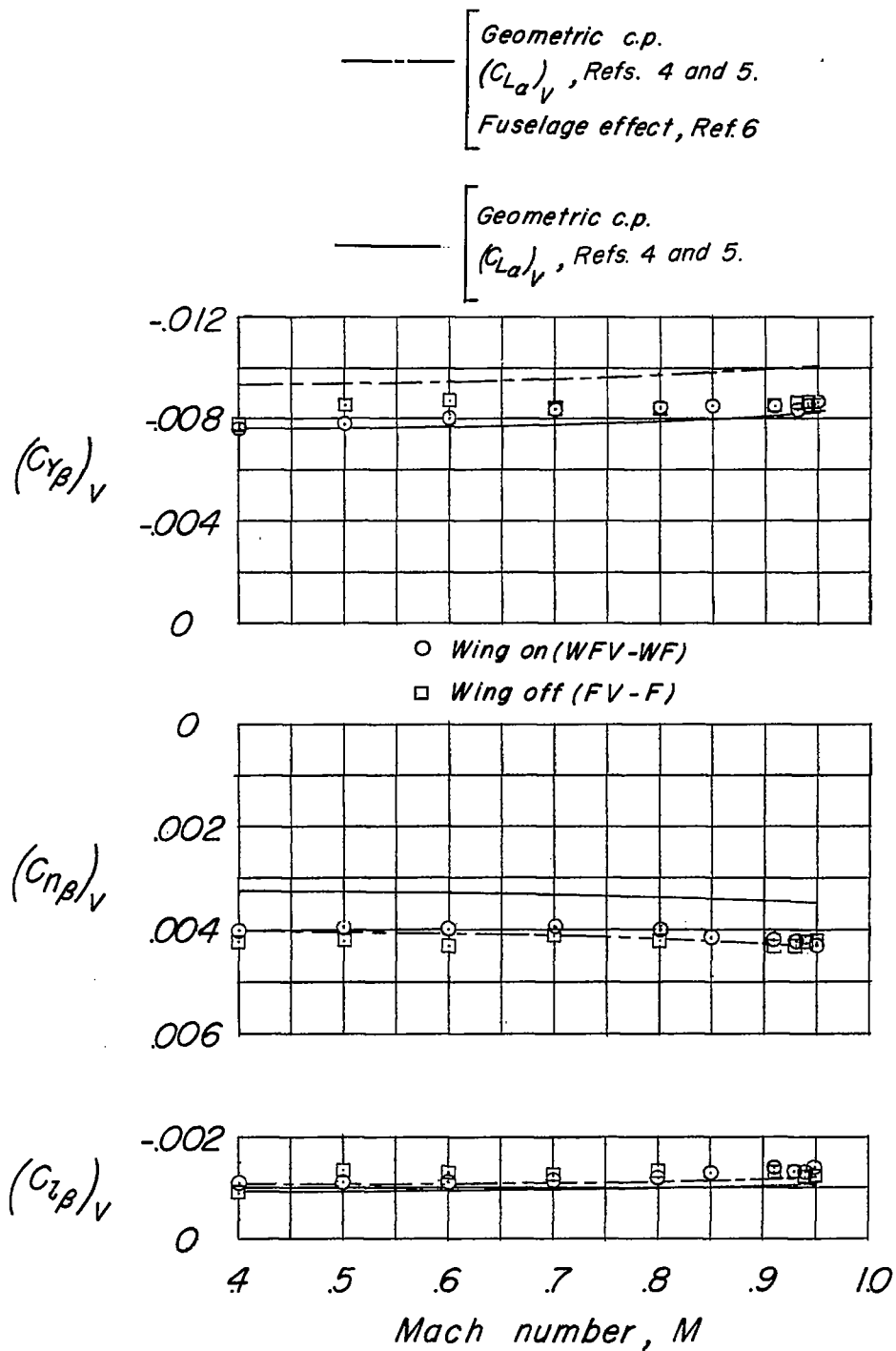
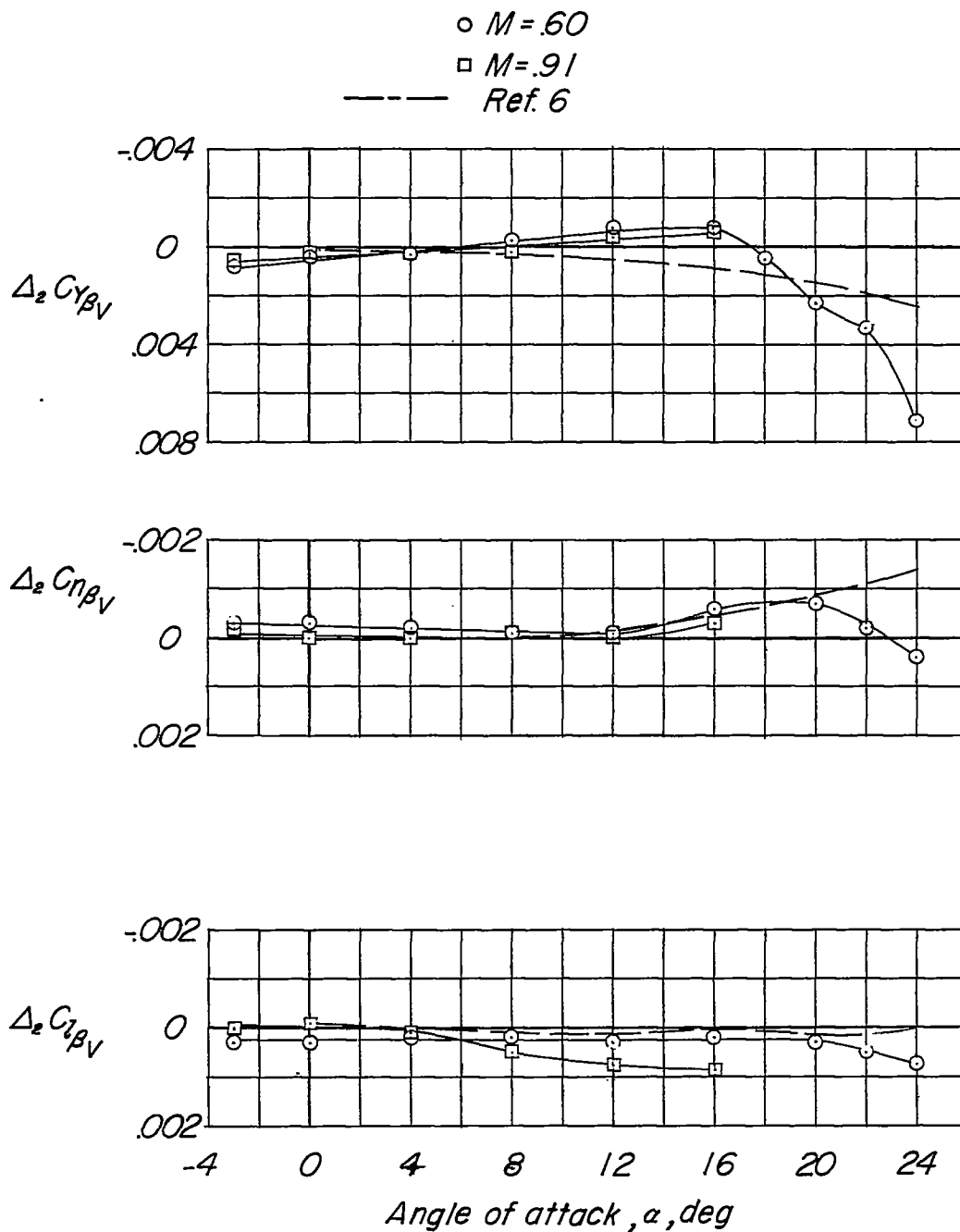
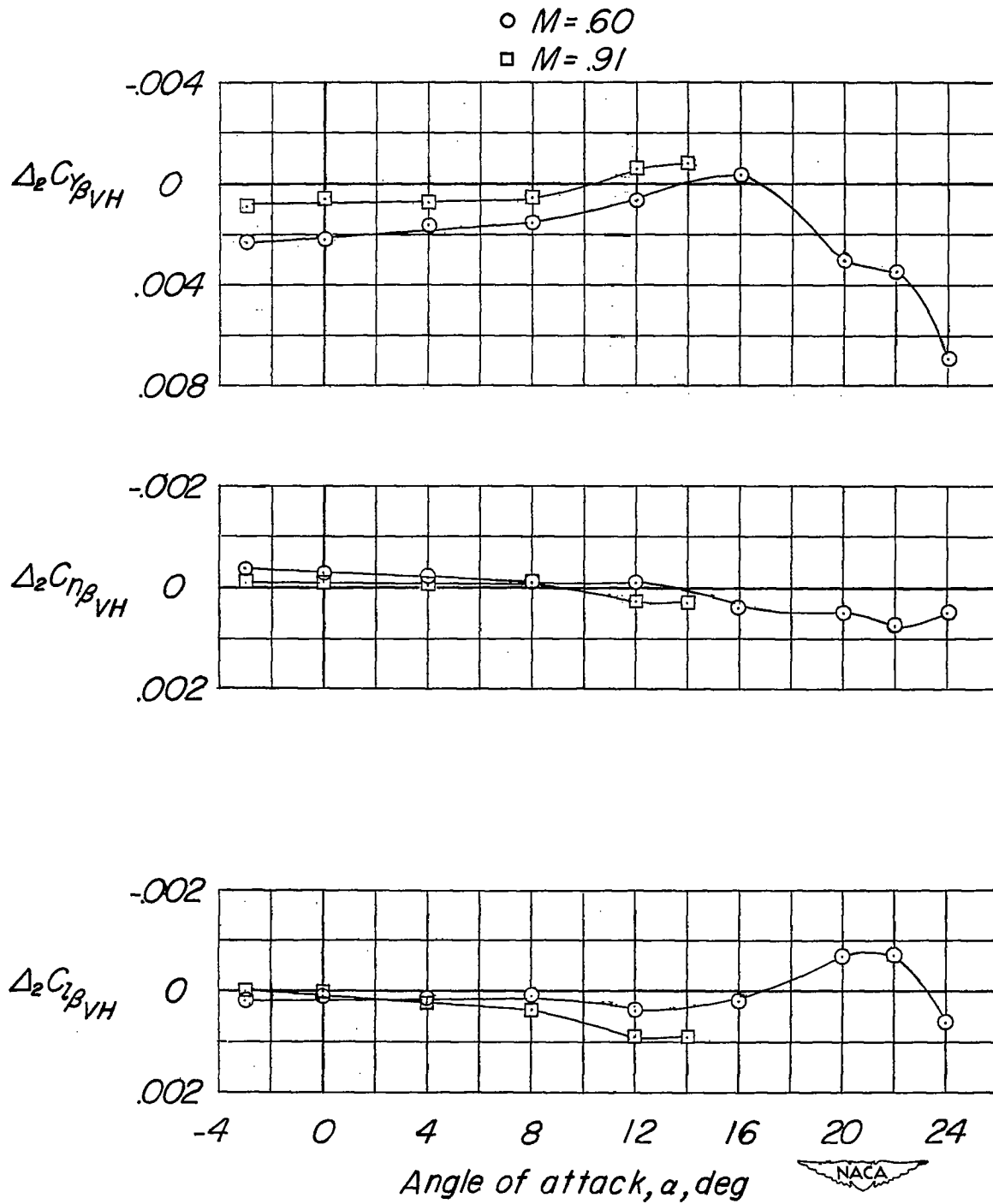


Figure 13.- Variation of the lateral-stability derivatives with Mach number compared with calculated variations. $\alpha = 0^\circ$.



(a) Vertical-tail contribution.

Figure 14.- Wing interference on the tail contributions to the lateral-stability derivatives.



(b) Contribution of the vertical- and horizontal-tail combination.

Figure 14.- Concluded.